RESEARCH ARTICLE

Porous Graphene Produced by Carbothermal Shock for Green Electromagnetic Interference Shielding in Both Microwave and Terahertz Bands

Congli Zhou, Kun Zhang, Xiao Sun, Xingchuan Zhao, Kaiwen Zheng, Jiawei Mi, Fangzhu Qing,* Qiye Wen,* and Xuesong Li*

The prospect of graphene-based shielding materials in the form of fillers is limited by the cumbersome preparation of graphene. Herein, defect-tunable porous graphene prepared by carbothermal shock using low-value sucrose as a precursor is proposed as an effective shielding filler. The resultant porous graphene exhibits 32.5 dB shielding efficiency (SE) and 2.5–18 GHz effective bandwidth at a mass loading of 20 wt%, competing with the shielding performance of graphene fillers prepared by other methods. Particularly, defect-rich graphene synthesized by increasing voltage and prolonging time shows increased electromagnetic (EM) wave absorption, echoing the current concept of green shielding. In addition, the strategy of controlling the discharge conditions to improve the absorption by the shield is developed in the terahertz band. The average SE and reflection loss of the samples in the THz band (0.2–1.2 THz) exhibit 40.7 and 15.9 dB at filler loading of 5 wt%, respectively, achieving effective shielding and absorption of THz waves. This work paves a new way for low-cost preparation of graphene for EM interference shielding fillers. Meanwhile, it supplies a reference for the shielding research of the upcoming applications integrating multiple EM bands (such as sixth-generation based integrated sensing and communication).

1. Introduction

Modern electronic devices have penetrated all areas of human life.[1] However, the accompanying electromagnetic interference (EMI) weakens the performance and reliability of electronic instruments and even affects human health. EMI shielding materials have been investigated to suppress the dilemma caused by electromagnetic (EM) radiation. Carbon materials and MXene have attracted great attentions with the advantages of chemical stability and low weight compared to metal-based EMI shielding materials.[2] Abundant shielding efforts involving carbon materials and MXene have emerged in the form of films,[3] foams,[4] fillers,[5] etc. Among them, EMI shielding fillers have a broad prospect because of the simple construction process and high utility rate of space. There are plentiful researches on fillers as shielding functional bodies, which involve fillers from zero to three-dimension and from single to multi-component.[4,6] Filler-based shields should have the necessary abilities: low filler loading to avoid agglomeration and high density, effective shielding performance including high shielding efficiency (SE) and wide effective bandwidth. However, the high SE value of the up-to-date filler-based shielding materials mainly results from reflection due to the high conductivity of fillers, while the growing research is concerned with promoting absorption to enhance SE (green EMI shielding).[7]

Among the carbon-based fillers that can basically achieve effective EMI SE values (>20 dB), graphene has excellent conductivity and high specific surface area (SSA) benefiting the formation of conductive network at low filler loading compared to other carbon materials while is much cheaper than MXene (**Table 1**). Various techniques for the production of graphene fillers have been developed, typically by physical exfoliation of graphite or reduction of graphene oxide (GO).[8] Many obstacles still exist with these top-down strategies such as the lack of control on defects, environmental issues due to the use of chemicals, and high cost with high energy input and time consuming. Recently, there was a report on preparation of graphene by carbothermal method, which converted carbon materials of low

C. Zhou, K. Zhang, X. Sun, X. Zhao, K. Zheng, F. Qing, Q. Wen, X. Li
State Key Laboratory of Electronic Thin Films and Integrated Devices
University of Electronic Science and Technology of China
610054, Chengdu, China
E-mail: qingfz@uestc.edu.cn; qywen@uestc.edu.cn; lxs@uestc.edu.cn

C. Zhou, K. Zhang, X. Zhao, K. Zheng F. Qing, X. Li
School of Integrated Circuit Science and Engineering
(Exemplary School of Microelectronics)
University of Electronic Science and Technology of China
610054, Chengdu, China

X. Sun, Q. Wen
School of Electronic Science and Engineering
University of Electronic Science and Technology of China
610054, Chengdu, China

J. Mi, F. Qing, Q. Wen, X. Li
Shenzhen Institute for Advanced Study
University of Electronic Science and Technology of China
518110, Shenzhen, China

The ORCID identification number(s) for the author(s) of this article can be found under https://doi.org/10.1002/smtd.202201493.

DOI: 10.1002/smtd.202201493

Table 1. EMI shielding performance of carbon-based composites.

Filler	Preparation of filler	Matrix	Filler loading [wt%]	d[a] [mm]	SE_T [dB]	TB[b] [GHz]	Ref.
Graphene	Chemical reduction	Epoxy	15	N/A[c]	21	8.2–12.4	[10]
Graphene	Functionalized with acid	PVDF	5	N/A	18	1–8	[11]
					20	8-12	
Graphene	Chemical reduction of GO	PU Foam	10	60	57.7	8–12	[12]
S-rGO	Annealing	N/A	100	0.14	33.2	0.1–4.0	[6i]
rGO	Chemical reduction	Wax	20	2	29.7	2–18	[13a]
Gr-220/300	Carbothermal shock of carbon	Wax	20	2	32.5	2.5–18	This work
Graphene foam	CVD	PDMS	0.8	1	≈30	0.03–1.5	[14]
					≈20	8–12	
Graphene (film)	Thermal reduction of GO	TPU	20	0.05	26	5.4–59.6	[15]
CB	Functionalized with acid	PANI/POX	10	N/A	19.9	8.2–12.4	[16]
CB	Heat treatment before use	ABS	35	1.5	6	0.2–1.6	[17]
MWCNT	Purchased	PLLA	10	2.5	23	8–12	[18]
3D-CNT	CVD	Epoxy	0.66	2	33	8–12	[19]
$Ti_3C_2T_x$	HF etching	Wax	60	2	39.1	2–18	[20]

[a]Sample thickness; [b]Bandwidth of the test; [c]Not available.

and/or negative value into graphene in an environment-friendly way with high energy conversion efficiency and short production time.[9] This method also has the advantage of controlling the degree of product defects in a large temperature range (>2000 K). By taking these advantages, we synthesized porous graphene from low-cost sucrose precursor via carbothermal shock within a few hundred milliseconds and investigated its application for EMI shielding. Except that the whole process is simple and requires no post-treatment, the porous structure and high electrical conductivity of the product enables SE value of 32.5 dB at 20 wt% filler loading and effective bandwidth covering 2.5–18 GHz, which is comparable to the composites with graphene as a single filler. In addition, extending the discharge time in carbothermal process raises the defect degree and moderates the conductivity, accompanied by the enhancement in synergy of conductive and polarization loss resulting in an increase of A coefficient (indicating the enhanced EM energy

attenuation by absorption). This strategy to enhance absorption is also demonstrated effective in terahertz (THz) band. Through the discharge control in carbothermal shock process, the transition from reflection to absorption for most EM waves is realized. The optimum average SE and reflection loss (RL) reaches 40.7 and 15.9 dB at a filler loading of 5 wt% correspondingly. Our work does not require further separation and purification of the obtained porous graphene. Competitive shielding performance can be achieved by simply blending the product with matrix.

2. Results and Discussion

The stepwise preparation of porous graphene was schematically illustrated in **Figure 1**. See details in the Experimental Section and Supporting Information. The scanning electron microscopy
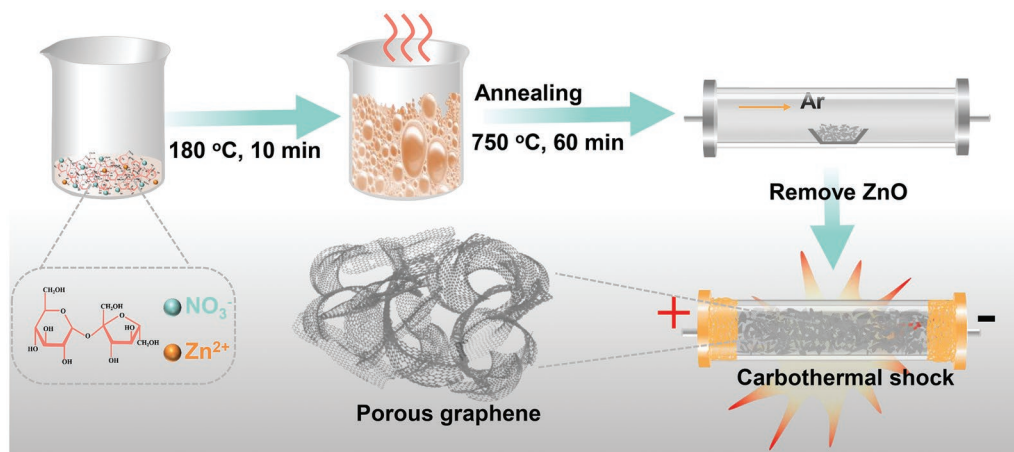

Figure 1. Schematic of the carbothermal synthesis of porous graphene.

**ADVANCED
SCIENCE NEWS**

www.advancedsciencenews.com

**small
methods**
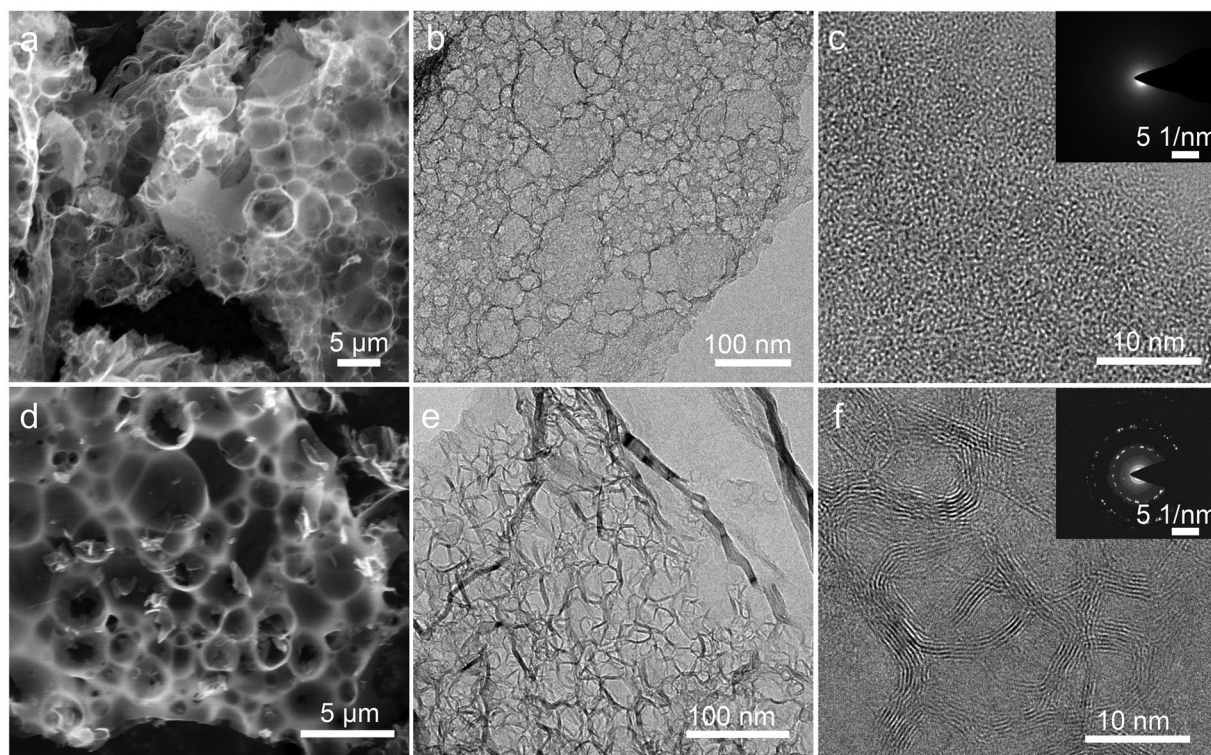
www.small-methods.com

Figure 2. SEM, TEM, and HRTEM images of a–c) PC and d–f) Gr-220/300, respectively. The insets in (c) and (f) show the corresponding SAED patterns.

(SEM) and transmission electron microscopy (TEM) images in **Figure 2** showed that Gr-220/300 retained the porous structure originating from porous carbon (PC). Here "Gr-220/300" is the label of a typical carbothermal synthetic porous graphene, where 220 denotes the discharge voltage with the unit of volt while 300 denotes the discharge time with the unit of millisecond (see Table S1, Supporting Information). In contrast, the as prepared Gr-220/300 differed from precursor PC in crystallinity as shown in the high-resolution TEM (HRTEM) images and selected area electron diffraction (SAED) patterns in Figure 2c,f, which revealed the transformation from amorphous PC to crystalline state, confirming that the pore skeletons of Gr-220/300 were composed of several layers of graphene.

Figure 3a shows the powder X-ray diffraction (XRD) characterization of PC and graphene, where Gr-220/300 exhibited extinct (002) peak around 26.3°, which was consistent with the crystallinity shown by its HRTEM. Raman spectroscopy is regarded as an effective way to characterize graphene.[21] From Figure 3b it could be seen that Raman spectrum of PC showed typical features of amorphous carbon with wide and overlapped D and G bands and low and spread 2D band. The transition from amorphous PC to graphene could be promoted by increasing the discharge voltage, e.g., from 150 to 180 to 220 V with a fixed discharge time of 300 ms as demonstrated by the increased sharp 2D band and the decrease of defect density as indicated by the intensity ratio of D to G bands (I_D/I_G). On the other hand, when the voltage was fixed at 220 V, I_D/I_G increased with the discharge time (Figure 3c). A possible reason may be that because the total energy is constant for a fixed voltage of a capacitor, the elongation of discharge

time widens the dispersion of energy over time and therefore lowers the peak temperature, resulting in worse crystallization of grpahene. X-ray photoelectron spectroscopy (XPS) characterization was performed on PC and Gr-220/300 (Figure 3d–f) to study the chemical state of the samples before and after carbothermal process. Zinc nitrate reacted with sucrose by heating (see Equation (S1), Supporting Information), the decomposed gas blew the molten sucrose into bubbles. The sucrose was further dehydrated and polymerized,[22] and the nitrogen element that was not volatilized in the form of gas was doped into the PC when the sugar was polymerized leading to the C 1s of PC was N-doped with a doping content of 3.30 at% (Figure S7 (Supporting Information), N was mainly doped as pyridinic, pyrrolic, and graphitic N). After undergoing flash heat during discharge, N was undetectable and O was decreased to ≈0.95 at%, (Figure 3d). The C 1s spectra of PC and Gr-220/300 (Figure 3e,f) demonstrated the decrease of oxygen-containing functional groups and the conversion of part of C—C sp³ to C—C sp². See Tables S2 and S3 (Supporting Information) for the the binding energy assignment. The N₂ adsorption–desorption isotherms and pore size distributions for PC and Gr-220/300 were shown in Figure 3g,h. Both contained micro and mesopores while the SSA decreased from 1184 m² g⁻¹ for PC to 503 m² g⁻¹ for Gr-220/300. A possible reason may be that the strong shock generated during the carbothermal process caused the rupture of nanopores in the PC (Figure 3h). Figure 3i showed the comparison of the electrical conductivity versus SSA of Gr-220/300 with other carbon materials. In general, conductivity and SSA are reversely correlated. From Figure 3i it could be seen that Gr-220/300 was superior to most
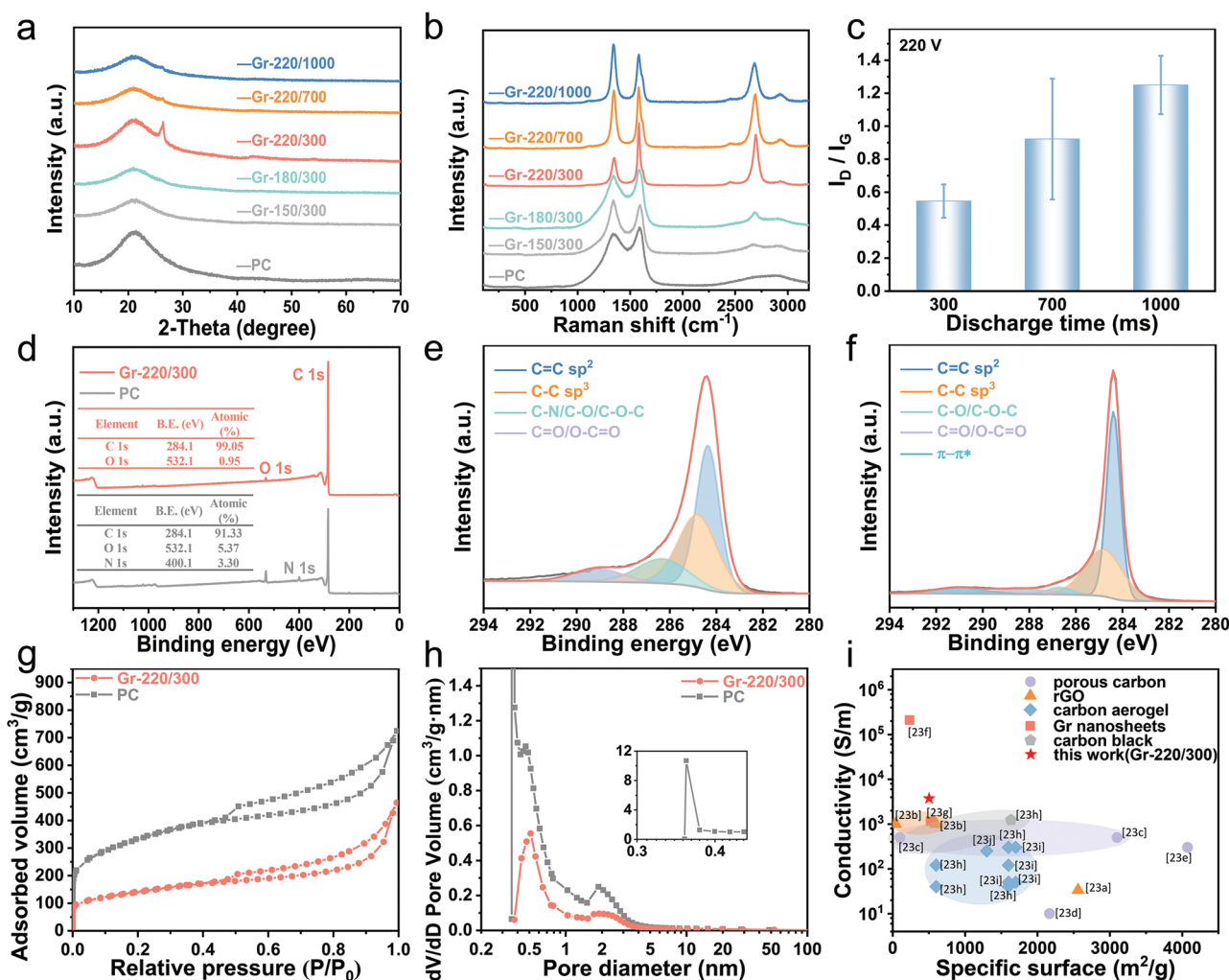
ADVANCED
SCIENCE NEWS
www.advancedsciencenews.com

small
methods
www.small-methods.com

Figure 3. a) XRD patterns and b) Raman spectra of PC and graphene with different discharge conditions. c) Average intensity ratio of D to G band (I_D/I_G) obtained by taking a scanning of 20×20 points with a step of 1 μm per point. d) XPS survey and e,f) high-resolution spectra for C1s on PC and Gr-220/300, respectively. g) BET N_2 adsorption–desorption isotherms and h) pore size distributions for PC and Gr-220/300, respectively. i) Comparison of the electrical conductivity versus SSA of Gr-220/300 with other carbon materials.[23]

of other carbon materials with its high SSA and conductivity in the plot, which made it conducive to the formation of conductive network at low filler loading.

Figure 4a shows the derived EMI SE. SE (often denoted as SE_T) values of graphene with different discharge conditions showed a positive correlation with both frequency and mass loading (Figure S14e,f, Supporting Information). Gr-220/300 showed the best SE_T performance with both a wide effective bandwidth of 2.5–18 GHz and high SE_T values while the maximum SE_T value could be up to 33.03 dB for the case of Gr-220/700. This is comparable to most of other carbon materials as shown in Table 1.

SE_T is usually divided into reflection (SE_R) and absorption (SE_A). Generally, the SE_T values are positively correlated to the conductivity of the materials (Equation (S12), Supporting Information). However, there was a steep increase of SE_A (and therefore SE_T) (Figure S17b, Supporting Information) for Gr-220/700 and Gr-220/1000, indicating that there were additional factors which strengthened the absorption or attenuation for EM energy.

Rather than comparing the values of SE_A and SE_R, A and R coefficient are more effective in evaluating the reflection and absorption of EM waves.[13] From Figure 4b it could be seen obviously that Gr-220/300 had the best wide band EMI shielding performance with the low T coefficient, which demonstrated ≈99.74% EM energy shielded (Figure S18, Supporting Information). However, the high SE_T was mainly due to reflection with the high R (Figure S17c, Supporting Information) values resulting from the excessive conductivity. With the decrease of conductivity, the reflection decreased as well, but the absorption increased, providing the opportunity for green EMI shielding.

To understand the shielding mechanism and the energy conversion of graphene composites, EM parameters were measured as shown in Figure S19 (Supporting Information). ε' and ε'' represent the storage and loss capacity of the medium for EM energy, respectively, and the loss tangent value of the dielectric constant ($\tan\delta_\varepsilon = \varepsilon''/\varepsilon'$) is commonly used to evaluate the capability of dielectric loss.[24] ε'' showed a downward trend, among which Gr-220/300 and Gr-220/700 exhibited significant higher

ADVANCED
SCIENCE NEWS

www.advancedsciencenews.com
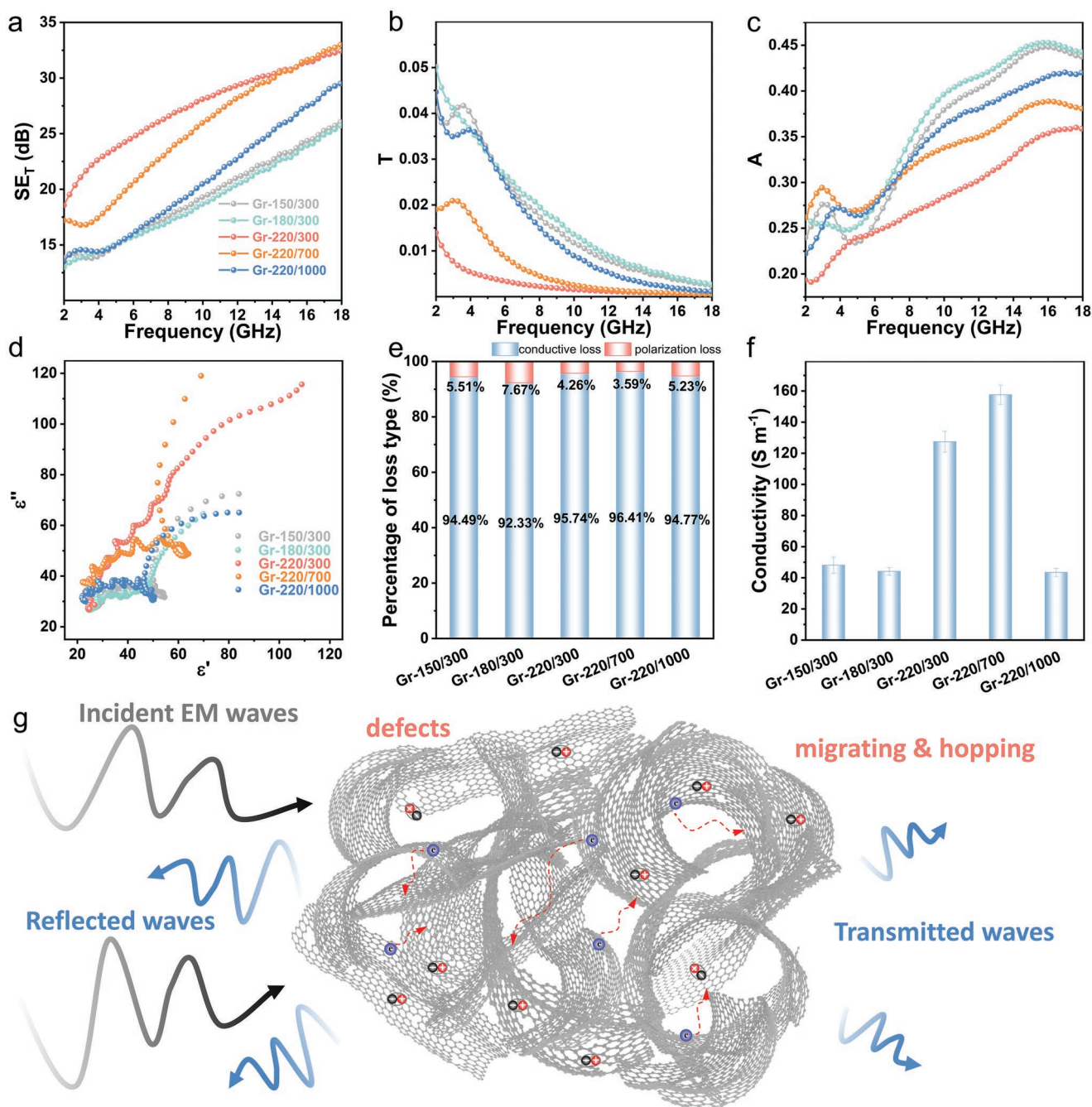
small
methods

www.small-methods.com

Figure 4. a) EMI SE_T, b) T, and c) A coefficient of graphene versus frequency. d) Cole–cole plot. e) Percentage of loss type of graphene samples prepared by different discharge conditions. f) Conductivity of graphene/wax composites. g) EMI shielding mechanism of the as-prepared graphene.

ε'' values than other samples due to their high electrical conductivity, which could be explained by Debye equations or free electron theory.[25] Gr-220/300 and Gr-220/700 also had high $\tan\delta_\varepsilon$ values, which indicated the high dielectric loss. Additionally, there were obvious resonance peaks in $\tan\delta_\varepsilon$ at high frequency indicating the existence of multiple polarization.[26] Cole–cole plot was investigated to study the dielectric properties. From Figure 4d it could be seen that Gr-220/300 showed a distinct straight tail regarding the contribution of conductive loss while the others displayed two large semicircles manifesting the

polarization relaxation behavior.[27] Actually, ε'' is considered to be the sum of ε_p'' relating to the polarization relaxation and ε_c'' associating with the conduction current (Equation (S13)–(S15)). To figure out the contribution of ε_p'' (polarization loss) and ε_c'' (conductive loss) on dielectric loss, the relaxation time (τ), electrical conductivity (σ), ε_p'', and ε_c'' were fitted by non-linear square fitting method.[28] From Figure 4e it could be seen that the conductive loss was still the main loss way for incident EM energy. In addition, the relative polarization loss increased with the increase of defects. It could be considered that the defects

and residual surface functional groups acted as polarization centers that strengthened the attenuation of EM wave energy,[5b] which might explain why SE_A of Gr-220/1000 rose at high frequency. Therefore, the shielding mechanism can be summarized as: the conductive surface causes reflection which brings high SE_R; the defects and residual functional groups lead to the polarization relaxation loss, and the porous structure promotes the migration and hopping of charge carriers promoting the conductive loss, both of which contribute to the high SE_A.

The porous graphene showed more promising performance in THz bands, as shown in **Figure 5**. The THz time-domain spectroscopy system was employed to measure the signal intensity of the reflected and transmitted THz waves (0.2–1.2 THz). As can be seen from the THz time-domain spectra, comparing to the signal in air, the transmitted THz intensity through all the composites showed obvious decline representing all of them realized the effective shielding (Figure 5b). Moreover, the reflection of THz signals remained in low ranges for the composites except 5Gr-220/330 (the numeric prefix represents the filler loading percentage) and 5Gr-220/700 due to their high conductivity. The transmittance (Figure 5d), reflectance (Figure 5e), and absorption (Figure 5f) were calculated based on the frequency-domain spectra, which was obtained by fast Fourier transform (FFT) of the time-domain spectra.[29] They visually showed that all the samples except 5Gr-220/300 and 5Gr-220/700 achieved low reflection and high absorption, manifesting that all samples except 5Gr-220/300 and 5Gr-220/700 realized absorption–dominant shielding for THz waves. The absorption could be over 90% while all reserving high average THz EMI SE_T of over 30 dB (Figure 5i). When filler loading of Gr-180/300 is 5 wt%, the optimal average SE_T of 40.7 dB and RL of 15.9 dB could be obtained simultaneously. An increased loading of all the samples from 5 to 20 wt% could significantly enhance the shielding performance (Figure S21–S25).

Therefore, the strategy to select materials for different application requirements can be concluded:

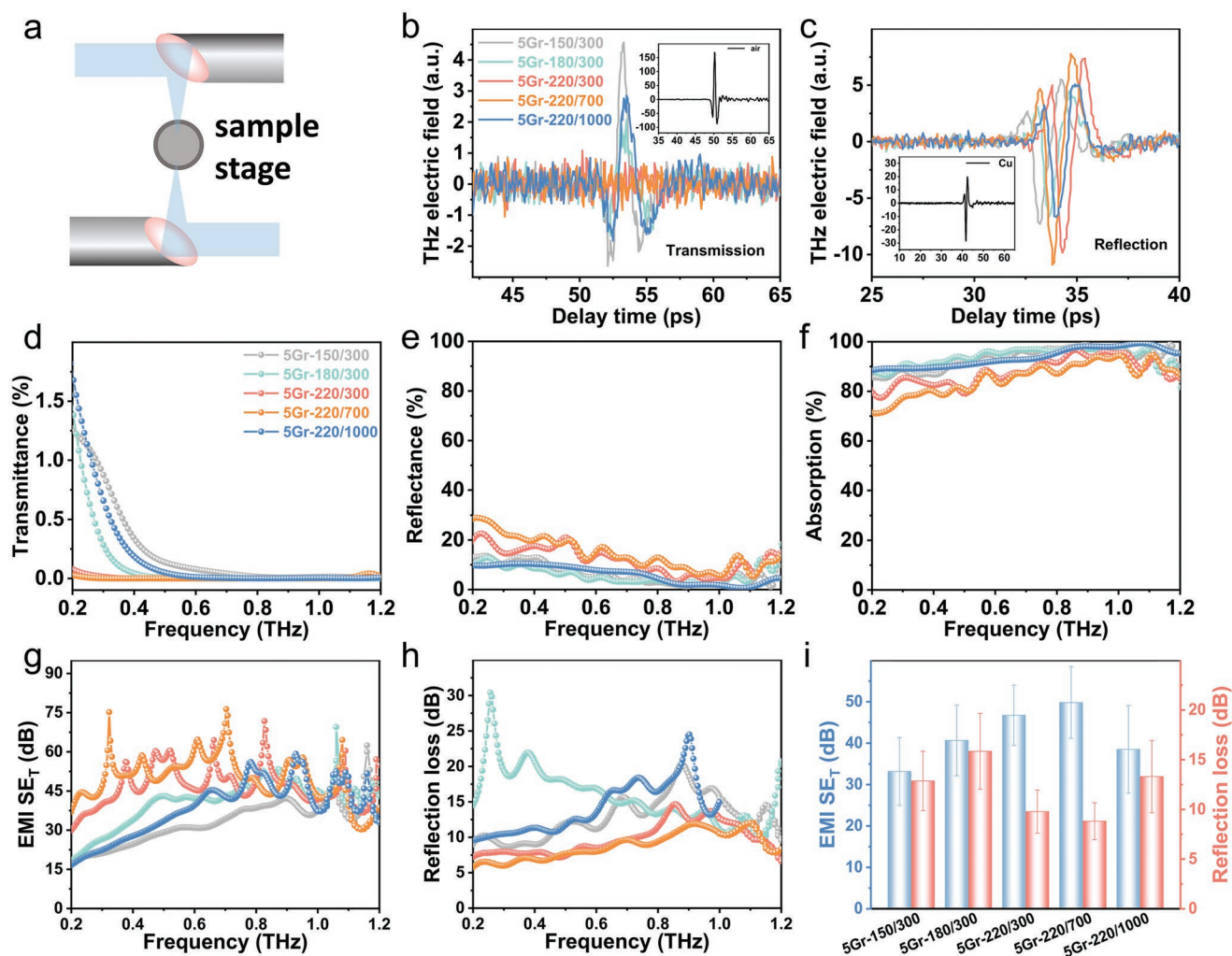1) High shielding in GHz bands requires enough loading of very conductive materials such as Gr-220/300 and Gr-220/700.

Figure 5. a) Schematic of the THz time-domain spectroscopy measurement. b) Transmission and c) reflection time-domain spectra of graphene/wax composites at filler loading of 5 wt%. The insets of (b) and (c) correspondingly showed the transmission intensity in air and reflection intensity of mirror. d) THz transmittance, e) reflectance, and f) absorption. g) EMI SE_T and h) RL versus frequency. i) Average SE_T and RL of different samples.

2) All can be used for THz shielding but low loading and low conductivity are preferred to achieve green shielding with high absorption.

3) Materials with moderate defects and conductivity such as Gr-180/300 and Gr-220/1000 can be used for an optimized green shielding in both GHz and THz bands.

3. Conclusion

In conclusion, porous graphene with tunable crystallinity was produced from low-value sucrose by carbothermal shock. The whole process is low-cost, simple, and environmentally friendly. The porous graphene was further demonstrated for good performance for green EMI shielding in both microwave and THz bands with high energy absorption, which is practically meaningful for some upcoming applications, such as sixth-generation based integrated sensing and communication that will adopt multiple electromagnetic bands.

4. Experimental Section

Sucrose, zinc nitrate hexahydrate, and hydrochloric acid (≥36 wt%) were purchased from Kelong Chemical Co., Ltd. (Chengdu, China). All reagents were of analytical grade and used without further purification. PC for the synthesis of porous graphene was prepared according to the melting sugar bubbling method.[22,30] Specifically, sucrose and zinc nitrate hexahydrate were mixed and ground at a mass ratio of 1:2. Then, the mixture was heated at 180 °C for 10 min on a hot stage in air and annealed at 750 °C (rising from room temperature to 750 °C at a rate of 5 °C min^{-1}) for 1 h under atmospheric pressure in Ar with a flow rate of 200 sccm in a tube furnace(The heating reaction of sucrose and zinc nitrate is shown in Equation (S1), Supporting Information). After that, the resulting black powders were soaked in 0.25 M HCl to remove the ZnO impurities. Finally, the precipitated porous carbon (PC) was filtered, washed with deionized water, and dried in an oven at 60 °C overnight for later use. Then the porous graphene was prepared by carbothermal shock.[9] Firstly, 60 mg PC was put in a quartz tube (length 50 mm, outer diameter 11 mm, inner diameter 8 mm), and the length of the material in the tube was between 1.50 and 1.75 cm (Table S1, Supporting Information). Then, the two ends of the quartz tube were plugged by copper electrodes, which were connected into the circuit (details were shown in Figure S1, Supporting Information) for carbothermal shock. After pretreatment of the sample and then the discharge treatment (150–220 V, 300–1000 ms), porous graphene powders were achieved (discharge details were shown in Table S1, Supporting Information).

Supporting Information

Supporting Information is available from the Wiley Online Library or from the author.

Acknowledgements

Conflict of Interest

The authors declare no conflict of interest.

Data Availability Statement

The data that support the findings of this study are available from the corresponding author upon reasonable request.

Keywords

[1] a) Y. Wu, J. Liu, S. Lin, K. Huang, E. Chen, K. Huang, M. Lei, *Eng. Sci.* **2022**, *18*, 105; b) R. Dilli, R. Chandra ML, D. Jordhana, *Eng. Sci.* **2021**, *16*, 308.

[2] a) F. Luo, D. Liu, T. Cao, H. Cheng, J. Kuang, Y. Deng, W. Xie, *Adv. Compos. Hybrid Mater.* **2021**, *4*, 591; b) N. Wu, B. Zhao, X. Chen, C. Hou, M. Huang, A. Alhadhrami, G. A. M. Mersal, M. M. Ibrahim, J. Tian, *Adv. Compos. Hybrid Mater.* **2022**, *5*, 1548; c) B. Dai, Y. Ma, F. Dong, J. Yu, M. Ma, H. K. Thabet, S. M. El-Bahy, M. M. Ibrahim, M. Huang, I. Seok, G. Roymahapatra, N. Naik, B. B. Xu, J. Ding, T. Li, *Adv. Compos. Hybrid Mater.* **2022**, *5*, 704.

[3] a) W. Zhao, H. Xu, J. Zhao, X. Zhu, Y. Lu, C. Ding, W. He, J. Bian, L. Liu, L. Ma, W. Wang, T. Zhou, X. Zhou, J. Li, S. Liu, Q. Zhao, *Chem. Eng. J.* **2022**, *437*, 135266; b) A. Iqbal, F. Shahzad, K. Hantanasirisakul, M.-K. Kim, J. Kwon, J. Hong, H. Kim, D. Kim, Y. Gogotsi, C. M. Koo, *Science* **2020**, *369*, 446.

[4] a) S. Liao, G. Li, X. Wang, Y. Wan, P. Zhu, Y. Hu, T. Zhao, R. Sun, C. Wong, *ACS Appl. Mater. Interfaces* **2022**, *14*, 3302; b) Y. Shen, Z. Lin, J. Wei, Y. Xu, Y. Wan, T. Zhao, X. Zeng, Y. Hu, R. Sun, *Carbon* **2022**, *186*, 9.

[5] a) V.-T. Nguyen, Q.-D. Nguyen, B. K. Min, Y. Yi, C.-G. Choi, *Chem. Eng. J.* **2022**, *430*, 133171; b) M.-S. Cao, X.-X. Wang, W.-Q. Cao, J. Yuan, *J. Mater. Chem. C* **2015**, *3*, 6589.

[6] a) H. Duan, H. Zhu, J. Yang, J. Gao, Y. Yang, L. Xu, G. Zhao, Y. Liu, *Composites, Part A* **2019**, *118*, 41; b) H. Lecocq, N. Garois, O. Lhost, P.-F. Girard, P. Cassagnau, A. Serghei, *Composites, Part B* **2020**, *189*, 107866; c) D. Munalli, G. Dimitrakis, D. Chronopoulos, S. Greedy, A. Long, *Composites, Part B* **2019**, *173*, 106906; d) Q. Jiang, X. Liao, J. Li, J. Chen, G. Wang, J. Yi, Q. Yang, G. Li, *Composites, Part A* **2019**, *123*, 310; e) N. Gill, V. Gupta, M. Tomar, A. L. Sharma, O. P. Pandey, D. P. Singh, *Compos. Sci. Technol.* **2020**, *192*, 108113; f) H. Jia, Q.-Q. Kong, Z. Liu, X.-X. Wei, X.-M. Li, J.-P. Chen, F. Li, X. Yang, G.-H. Sun, C.-M. Chen, *Composites, Part A* **2020**, *129*, 105712; g) Y. Chen, H.-B. Zhang, M. Wang, X. Qian, A. Dasari, Z.-Z. Yu, *Compos. Sci. Technol.* **2017**, *152*, 254; h) R. Kumar, S. Sahoo, E. Joanni, R. K. Singh, W. K. Tan, K. K. Kar, A. Matsuda, *Carbon* **2021**, *177*, 304; i) F. Shahzad, P. Kumar, S. Yu, S. Lee, Y.-H. Kim, S. M. Hong, C. M. Koo, *J. Mater. Chem. C* **2015**, *3*, 9802.

[7] a) D.-Q. Zhang, T.-T. Liu, J.-C. Shu, S. Liang, X.-X. Wang, J.-Y. Cheng, H. Wang, M.-S. Cao, *ACS Appl. Mater. Interfaces* **2019**, *11*, 26807; b) X.-X. Wang, J.-C. Shu, W.-Q. Cao, M. Zhang, J. Yuan, M.-S. Cao, *Chem. Eng. J.* **2019**, *369*, 1068; c) P. He, M.-S. Cao, Y.-Z. Cai, J.-C. Shu, W.-Q. Cao, J. Yuan, *Carbon* **2020**, *157*, 80; d) X. Jia, Y. Li, B. Shen, W. Zheng, *Composites, Part B* **2022**, *233*, 109652.

[8] K. M. Wyss, D. X. Luong, J. M. Tour, *Adv. Mater.* **2022**, *34*, 2106970.

[9] D. X. Luong, K. V. Bets, W. A. Algozeeb, M. G. Stanford, C. Kittrell, W. Chen, R. V. Salvatierra, M. Ren, E. A. McHugh, P. A. Advincula, Z. Wang, M. Bhatt, H. Guo, V. Mancevski, R. Shahsavari, B. I. Yakobson, J. M. Tour, *Nature* **2020**, *577*, 647.

[10] J. Liang, Y. Wang, Y. Huang, Y. Ma, Z. Liu, J. Cai, C. Zhang, H. Gao, Y. Chen, *Carbon* **2009**, *47*, 922.

[11] V. Eswaraiah, V. Sankaranarayanan, S. Ramaprabhu, *Macromol. Mater. Eng.* **2011**, *296*, 894.

[12] B. Shen, Y. Li, W. Zhai, W. Zheng, *ACS Appl. Mater. Interfaces* **2016**, *8*, 8050.

[13] a) B. Wen, X.-X. Wang, W.-Q. Cao, H.-L. Shi, M.-M. Lu, G. Wang, H.-B. Jin, W.-Z. Wang, J. Yuan, M.-S. Cao, *Nanoscale* **2014**, *6*, 5754; b) Q. Qi, L. Ma, B. Zhao, S. Wang, X. Liu, Y. Lei, C. B. Park, *ACS Appl. Mater. Interfaces* **2020**, *12*, 36568; c) M. Peng, F. Qin, *J. Appl. Phys.* **2021**, *130*, 225108.

[14] Z. Chen, C. Xu, C. Ma, W. Ren, H. M. Cheng, *Adv. Mater.* **2013**, *25*, 1296.

[15] B. Shen, Y. Li, D. Yi, W. T. Zhai, X. C. Wei, W. G. Zheng, *Carbon* **2017**, *113*, 55.

[16] A. Kausar, *Int. J. Mater. Chem.* **2016**, *6*, 6.

[17] X. Wang, *J. Electromagn. Anal. Appl.* **2011**, *03*, 160.

[18] T. Kuang, L. Chang, F. Chen, Y. Sheng, D. Fu, X. Peng, *Carbon* **2016**, *105*, 305.

[19] Y. Chen, H.-B. Zhang, Y. Yang, M. Wang, A. Cao, Z.-Z. Yu, *Adv. Funct. Mater.* **2016**, *26*, 447.

[20] X. Liu, J. Wu, J. He, L. Zhang, *Mater. Lett.* **2017**, *205*, 261.

[21] J.-B. Wu, M.-L. Lin, X. Cong, H.-N. Liu, P.-H. Tan, *Chem. Soc. Rev.* **2018**, *47*, 1822.

[22] C. Wang, M. J. O'Connell, C. K. Chan, *ACS Appl. Mater. Interfaces* **2015**, *7*, 8952.

[23] a) B. Xu, H. Wang, Q. Zhu, N. Sun, B. Anasori, L. Hu, F. Wang, Y. Guan, Y. Gogotsi, *Energy Storage Mater.* **2018**, *12*, 128; b) W. S. Hummers Jr., R. E. Offeman, *J. Am. Chem. Soc.* **1958**, *80*, 1339; c) Y. Zhu, S. Murali, M. D. Stoller, K. J. Ganesh, W. Cai, P. J. Ferreira, A. Pirkle, R. M. Wallace, K. A. Cychosz, M. Thommes, D. Su, E. A. Stach, R. S. Ruoff, *Science* **2011**, *332*, 1537; d) X. Geng, L. Li, M. Zhang, B. An, X. Zhu, *J. Environ. Sci.* **2013**, *25*, S110; e) V. B. Mohan, R. Brown, K. Jayaraman, D. Bhattacharyya, *Mater. Sci. Eng., B* **2015**, *193*, 49; f) A. R. Kamali, *J. Ind. Eng. Chem.* **2017**, *52*, 18; g) A. R. Kamali, J. G. Yang, Q. Sun, *Appl. Surf. Sci.* **2019**, *476*, 539; h) D. Pantea, H. Darmstadt, S. Kaliaguine, C. Roy, *Appl. Surf. Sci.* **2003**, *217*, 181; i) L. Zhang, X. Zhao, *Chem. Soc. Rev.* **2009**, *38*, 2520; j) V. Skákalová, P. Kotrusz, M. Jergel, T. Susi, A. Mittelberger, V. Vretenár, P. Šiffalovič, J. Kotakoski, J. C. Meyer, M. Hulman, *J. Phys. Chem. C* **2017**, *122*, 929.

[24] Y. Wang, X. Di, J. Chen, L. She, H. Pan, B. Zhao, R. Che, *Carbon* **2022**, *191*, 625.

[25] J. Xi, E. Zhou, Y. Liu, W. Gao, J. Ying, Z. Chen, C. Gao, *Carbon* **2017**, *124*, 492.

[26] Y. Qiu, H. Yang, Y. Cheng, Y. Lin, *Composites, Part A* **2022**, *154*, 106772.

[27] G. Cheng, F. Pan, X. Zhu, Y. Dong, L. Cai, W. Lu, *Compos. Commun.* **2021**, *27*, 100867.

[28] a) H. Xu, X. Yin, M. Li, F. Ye, M. Han, Z. Hou, X. Li, L. Zhang, L. Cheng, *Carbon* **2018**, *132*, 343; b) T. Li, D. Zhi, Y. Chen, B. Li, Z. Zhou, F. Meng, *Nano Res.* **2020**, *13*, 477.

[29] a) W. Shui, J. Li, H. Wang, Y. Xing, Y. Li, Q. Yang, X. Xiao, Q. Wen, H. Zhang, *Adv. Opt. Mater.* **2020**, *8*, 2001120; b) H. Wan, N. Liu, J. Tang, Q. Wen, X. Xiao, *ACS Nano* **2021**, *15*, 13646.

[30] a) W. Yang, D. Peng, H. Kimura, X. Zhang, X. Sun, R. A. Pashameah, E. Alzahrani, B. Wang, Z. Guo, W. Du, C. Hou, *Adv. Compos. Hybrid Mater.* **2022**, *5*, 3146; b) C. Hou, W. Yang, H. Kimura, X. Xie, X. Zhang, X. Sun, Z. Yu, X. Yang, Y. Zhang, B. Wang, B. B. Xu, D. Sridhar, H. Algadi, Z. Guo, W. Du, *J. Mater. Sci. Technol.* **2023**, *142*, 185.